Online Measurement of Voltage Gradient Distortion and Leakage Current of Heavily Contaminated Outdoor Insulation using Thermal Imaging

M. Albano, *Member, IEEE*, R.T. Waters, M. A. Slama, and A. Haddad, *Member, IEEE*

***Abstract*— A new thermal model of an insulator heat loss coefficient proves that evaporation power loss is more significant than thermal conduction to a moist environment. Consequently, the leakage current in a moist pollution layer may cause dry-band formation. Such bands are bridged and sustained by streamer discharges, which can initiate partial arcing. Clean-fog tests of contaminated insulators have been shown to provide infrared temperature data for the model, and the evaluation of voltage gradients in this dry-band regime. The same modelling also offers a unique method of online leakage current monitoring.**

***Index Terms*—Polluted insulator testing, temperature monitoring, evaporation modelling.**

I. INTRODUCTION

THE wetted surface of a polluted insulator has a typical leakage conductance of a few microsiemens. This enables dry bands to divide the pollution layer because a leakage current of a few milliamperes in magnitude promotes evaporation from the thin moist layer [1]. The voltage difference across such bands, following their loss of conductivity, is sufficient to initiate electrical breakdowns that bridge the bands. These take the form of corona streamers (Figure 1(a) [1]) that are of low luminosity mainly in the ultraviolet (UV) spectral range. The streamer initiation across a dry band reduces the leakage current below that which was present prior to the band formation and causes negligible damage to the insulator. Nevertheless, the local energy dissipated by the streamers is shown by the infrared record to heat the insulator surface (Figure 1(b)) which will prevent rewetting and so conserve the band. The temperature rise associated with dry-band formation is modest. In this case, where the insulator is in a clean fog environment at 14°C, yet much of its surface is at 16°C and the dry bands can reach 26-27°C.

Although dry band formation initially reduces the leakage current, it also introduces regions of high electric stress on the insulator surface. These are observed to be able to initiate transient partial arcs as shown in fog chamber photography (Figure 1(c)). The peak currents of partial arcs may become two orders greater than those of the dry-band corona streamers. Although consequent insulator flashover is rare if a sufficient surface creepage distance is specified, partial arc damage may significantly reduce the service life of polymeric materials even where filler materials have been incorporated. Online assessment of the condition of live high voltage electrical insulation by commercial UV or infrared (IR) photography is available. Recent research has shown that ultrasonic signals [2] may also provide a qualitative assessment of breakdown activity and predict degradation and imminent faults.

An increase of pre-flashover leakage current would be a better symptom of insulator problems, but data are difficult to acquire on live-line systems. However, quantitative online temperature assessment using IR thermal data is also a more direct parameter and is shown in this paper to measure the voltage gradient distortion caused by dry banding that can occur in the polluted, moist conditions of marine, industrial or desert environments. The consequent increase of leakage current by partial arcing can also be obtained. This thermal model requires the evaporation process from insulators to be calculated, which has never before been numerically modelled because classical kinetic theory can be complex to quantify (Section IV.A). This difficulty is overcome here using the Bowen Ratio [3], a factor which evaluates the ratio of the total thermal losses to the latent-heat losses. In order to avoid kinetic theory modelling, Bowen [3] envisaged that, although latent-heat energy is directly abstracted at any evaporating wet surface, the rate of that loss can be treated analytically when the evaporated molecules are then physically transported into the surrounding gaseous environment (Section IV.B). In this first application of the Bowen Ratio to high-voltage technology (Section V and Appendix 1) the quasi-steady-state boundary condition for evaporation is the constantly wetted insulator surface. Its temperature will vary longitudinally but will everywhere be

M. Albano, R.T. Waters, and A. Haddad are with Advanced High Voltage Engineering Research Centre, Cardiff University, Queen's buildings, 15-17 The Parade, Cardiff, CF24 3AA, Wales, UK (e-mail: albanom@Cardiff.ac.uk).

M. A. Slama was with Advanced High Voltage Engineering Research Centre, Cardiff University, UK. He is now with IRT Saint Exupéry, 31405 Toulouse, France

higher than that of the saturated fog or rain environment.

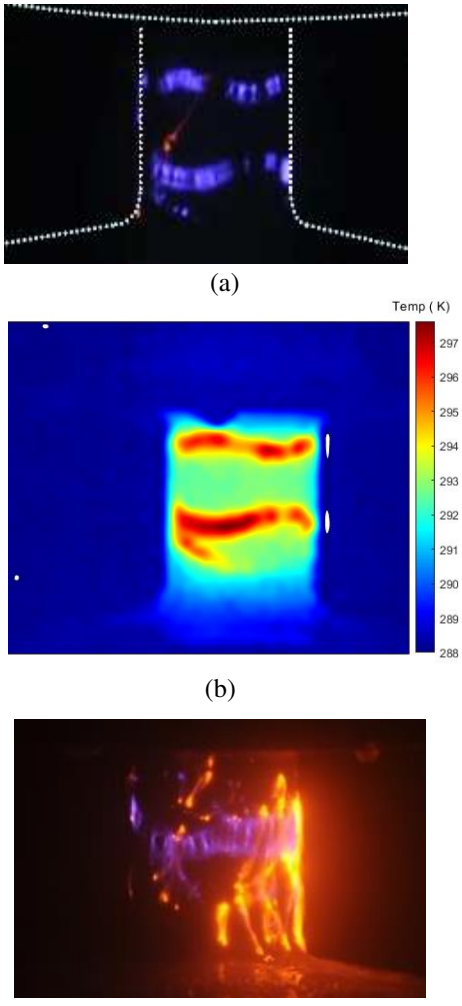

Fig. 1. Dry bands and partial arcs on the trunk section of a silicone rubber insulator. Simultaneous (a) visible and (b) infrared images of dry band streamers. (c) Partial-arc inception and bridging of a dry band [1].

II. INSULATOR PROFILE AND CLEAN_FOG TESTS

A demonstration of the implementation of the model will utilize laboratory fog-chamber tests on polluted silicone-rubber insulators (Sections II and V) comprising leakage current measurements synchronized with visual recording and IR temperature data [4, 5].

Figure 1 was obtained with four-shed, three-trunk 11kV insulators (Table I and Figure 2) using silicone-rubber formulations, to which a layer of salt deposit density 0.64mg/cm^2 was applied. A low-voltage test before dry-band formation indicated a leakage resistance of 1MΩ. High-voltage tests in a clean-fog pollution test chamber used a 150 kVA source of suitable rating to supply a linear ramp test voltage of 4 kV/minute.

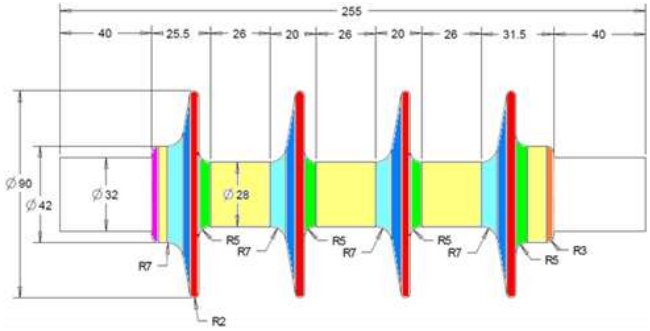

Fig. 2. Test insulator design.

TABLE I
11 KV TEST INSULATOR DIMENSIONS (FIG.1)

Creepage distance (L)	375mm
Trunk diameter (d)	28mm
Trunk length (T)	35mm
Shed diameter (D)	90mm
Axial length (l)	175mm
Form factor (F) (Appendix A.1)	2.76

These tests enabled the acquisition and post-processing of both voltage and leakage current data with a synchronized video recording [1, 4-5]. In addition, continuous IR recording [1] with a FLIR A325 camera of spectral range from 7.5 to 13μm and an image resolution of 320 x 240 pixels was of maximum frame frequency 60 Hz. The precision of the IR temperature measurement in the fog environment was calibrated to be ± 0.5°C in the temperature range 0-50°C.

A Nikon D700 digital camera with 200mm focal length and long exposure time also enabled the low-luminosity dry-band streamer discharges to be detected.

III. THERMAL MODELLING

A. Leakage Current and Voltage Gradients Before Dry Band Formation

The longitudinal distribution of the voltage gradient E(x) associated with a small leakage current I_L before dry-band formation, in a uniform moist pollution layer of conductance k (S) (the product of the layer conductivity (S/m) and the layer thickness) over the insulator creepage distance L, is

$$E(x) = \frac{I_L}{k\,\pi D(x)}. \quad (1)$$

Here D(x) is the diameter of the cross-section at any longitudinal surface location 0 < x < L along the creepage path. If the voltage across the insulator is U, the value of a constant layer conductance can be obtained by integration over the surface creepage length:

$$k = [I_L/U] \int_0^L dx/\pi D(x) = I_L F / U \quad (2)$$

Here, the integral term is defined to be the insulator form factor F, which is further utilized in the form factor calculation of each section of the insulator as discussed below. The longitudinal variation of the per-unit surface voltage gradient E(x) over the creepage distance will, in this case, be defined solely by the insulator geometry:

$$\overline{E(x)} = \frac{E(x)}{U} = 1/[F\pi D(x)] \quad (3)$$

For the test insulator of Table I, the profile of E(x) over the creepage distance is calculated in section V (blue curve). Before dry-band distortion occurs, the gradient at the trunk sections of this insulator is shown to be sixfold greater than the mean gradient on the sheds. In consequence, a leakage current of a few milliamperes will cause dry-band formation and voltage gradient distortion to occur exclusively on the insulator trunks.

B. Voltage Gradients after Dry-Band Formation

A non-uniform and reduced layer conductance k(x) will result from the evaporation that creates dry-band formation, so that an alternative approach is needed to determine the distributions of the modified surface voltage gradient $E_M(x)$ and the leakage current density J(x), especially for the dry-band areas. For this purpose, the analysis will utilize measurements of the temperature differences θ(x) between the pollution layer temperature variation $T_S(x)$ and the ambient temperature T_A in the fog. A heat loss function f[θ(x)] will represent the equality of the local input power per unit area $P_I(x)$ associated with the leakage current, with the heat-loss processes governing the power dissipation per unit area $P_H(x)$:

$$f[\theta(x)] = P_I(x) = J(x)\, E_M(x) = P_H(x) \quad (4)$$

The modified voltage gradient $E_M(x)$ at the location x will no longer depend solely upon the insulator geometry and the leakage current, but also upon the heat loss function. Equations (3) and (4) then give

$$E_M(x) = \frac{f[\theta(x)]}{J(x)} = \frac{\pi D(x)\, f[\theta(x)]}{I_L} = \frac{f[\theta(x)]}{F\,\overline{E(x)}\, I_L} \quad (5)$$

The voltage gradients $E_M(x)$ created by dry bands will be shown in Section V to be significantly greater than the pre-dry-band gradients E(x). Since the procedure utilizes thermal profiles from infrared records and physical modelling of the heat loss function per unit area f[θ(x)], it is necessary to quantify all three heat loss mechanisms, viz. conduction to the insulator body and the gaseous environment, radiation, and latent heat loss by evaporation:

$$f[\theta(x)] = P_H(x) = P_I(x) = P_{CC}(x) + P_R(x) + P_E(x) \quad (6)$$

C. Conduction Power Loss

The fog tests employed spray nozzles under compressed air, which produced forced convection of water droplets, so that the water content of the pollution layer was continuously replenished by droplets at ambient fog temperature. Classical Newton heat coefficients h (Equation (7)) and H (Equation (14), Section IV) will respectively define the associated power loss/unit area by conduction both to the insulator body and to the gaseous environment.

$$P_{CC}(x) = h\,\theta(x) \quad (7)$$

This heat transfer coefficient h ($W/m^2/K$) for is governed by the insulator structure. In the present work, the environmental coefficient H is experimentally determined from the fog test data (Section 4).

D. Radiation Power Loss

Stefan's Law gives the net radiation loss/unit area from a surface of emissivity ε, at an absolute temperature $T_S(x)$, in an environment at an absolute temperature T_A:

$$P_R(x) = \varepsilon\sigma(T_S(x)^4 - T_A^4) \quad (8)$$

Here $\sigma = 5.67\ 10^{-8}\ W/m^2K^{-4}$ and $0 < \varepsilon < 1$. The temperature rise associated with dry-band formation is modest (Section V), for a polluted insulator in a clean-fog environment at 14°C. Most of its surface is typically at 22°C, and the dry bands are at 26-27°C. At the absolute temperature scale, these temperature differences of $\theta(x) = T_S(x) - T_A << T_A$ so that the radiation loss/unit area (W/m^2) is closely approximated by

$$P_R(x) = 4\,\varepsilon\,\sigma\,T_A^3\,\theta(x) \quad (9)$$

The combined power loss/unit area from conduction and radiation is then

$$P_{CC}(x) + P_R(x) = (h + H + 4\,\varepsilon\,\sigma\,T_A^3)\,\theta(x) \quad (10)$$

For an ambient temperature of 290 K and an emissivity of 0.9, the Newton heat transfer coefficient h is thus increased by 5 $W/m^2/K$ by radiation. In other examples such as air cooling, h ≈ 10-100 $W/m^2/K$, and the radiation contribution may not be negligible. In water-spray cooling of hot surfaces, thermal losses of 100 W/m^2 or more are achieved.

E. Evaporation Power Loss

Equality of the evaporation rate R_{max} from the insulator surface with the wetting rate w (kg/m^2s) is the initial condition to create a dry band. The leakage current will fall, and the remaining insulator surface will remain moist with a lower evaporation rate. In the fog test examples of Section V, the maximum rate of water injection was 8l/h, which was continuously removed over the wet-chamber inner surface of approximate area $24m^2$. For this average wetting rate of approximately 100 $mg/m^2/s$, the evaporation power loss/unit area by latent heat (L_E = 2.26 MJ/kg) from the dry bands would be

$$P_E(max) = R_{max}\, L_E = w\, L_E \approx 200\ W/m^2 \quad (11)$$

However, the evaporation rates R(x) over the insulator surface will be lower and governed by the insulator profile and the vapour-pressure variation close to its surface. The evaluation of R(x) is key to the present thermal modelling and the calculation of the evaporation power loss $P_E(x)$ over the insulator. This is

addressed in Section IV and together with the evaluation of R(x) in relation to dry band formation in Section V.

IV. BOWEN MODEL OF EVAPORATION HEAT LOSS

A. Limitations of Kinetic Theory of Evaporation Rate

The specific evaporation rate G, i.e., the rate of loss of mass per unit area from an evaporating surface, is described by the Hertz-Knudsen equation, and has been verified by experiments with a range of organic liquids [5]. The equation in SI units is

$$G = (M/2\pi R)^{0.5} [\ p_L / T_L^{0.5} - p_E / T_E^{0.5}\ ] \text{ kg/m}^2\text{s} \qquad (12)$$

Here, p_L and p_E (Pa) are the saturated vapour pressure values, which are present immediately above the surface of the evaporating liquid at a temperature T_L (K), and in the environment at temperature T_E into which the evaporation occurs. M (kg/mol) is the molar mass of the liquid, and R = 8.314 (Pa m^3)/(K mol) is the Universal Gas Constant. A serious difficulty arises with this classical equation for polar molecules, such as H_2O, where the measured rate of evaporation is much smaller ($\leq$ 4%) than that predicted by (12). Later works [6,7] show that this difficulty is caused by an inadequate representation of the liquid state for these compounds. The expression of Eq. (12) requires inclusion of an evaporation coefficient ε_e that is physically based upon the fraction of molecules, in a Maxwell-Boltzmann energy distribution, with sufficient velocity to leave the liquid surface. The low value of ε_e together with its sensitivity to surface conditions and temperature severely limits the practical usefulness of (12) in the calculation of water evaporation rates.

B. Molecular Diffusion and the Bowen Concept of Latent-Heat Energy Transport by Water Molecules in Air

In order to circumvent this difficulty of calculating the rate of evaporation from kinetic theory, Bowen [3] demonstrated that P_E can be expected to be linearly related to the rate of thermal heat loss P_{CC} by conduction and convection to the gaseous environment because the comparative magnitude of these two heat loss processes will be similarly dependent on local conditions. This linear relationship has long proved invaluable for applications in heat transfer technology involving evaporation [8]. The following Sections propose for the first time the application of the Bowen concept to the dry-band process of water evaporation from polluted insulators.

The factor which has become known as the Bowen Ratio (B) defines the ratio of the heat losses per unit area from a wet surface that are caused respectively by conduction (with convection if present) and by evaporation, i.e.

$$B = P_{CC} / P_E \qquad (13)$$

The physical basis of the calculation of the Bowen ratio which will be used here is as follows:

The evaporation of each water molecule requires the expenditure of energy in the form of a latent heat loss which results in cooling of the liquid surface. The rate of energy loss is a product of the rate of evaporation and the latent heat of evaporation of the liquid. In a radical alternative to the kinetic theory approach, Bowen modelled this power loss on a novel basis: although the latent heat energy loss from the liquid occurs at the instant of evaporation, he recognized that steady-state evaporation is sustained if each evaporated molecule moves away from the surface and effectively transports the latent heat energy change away from the water surface by diffusion or convection. In this situation, these molecules can be assigned a notional energy density ϕ which will have a maximum value at the liquid-gas interface, and which will decrease with the H_2O molecular density as they diffuse into the cooler gas. Bowen could then compare this notional latent-heat energy transport process to the actual process by which a liquid surface loses thermal energy by conduction through the gas, where the thermal energy loss is truly transported by the gas molecules. The conducted thermal energy density τ has a maximum value given by the product of the gas number density and specific heat, and the temperature rise of the gas at the liquid surface.

The thermal power loss H and evaporation power loss λ to the environment is, on the Bowen concept, proportional to the rates of transport of the energy densities ϕ and τ, which in a still gas will depend respectively upon the diffusion velocities of the evaporated liquid molecules and of the heated air molecules. Then, in a z-direction normal to the liquid surface,

$$H = \frac{d\tau}{dt} = \frac{d\tau}{dz} \cdot \frac{dz}{dt} = \frac{Dgas}{z} \cdot \frac{d\tau}{dz} \qquad (14)$$

and

$$\lambda = \frac{d\phi}{dt} = \frac{d\phi}{dz} \cdot \frac{dz}{dt} = \frac{Dvapour}{z} \cdot \frac{d\phi}{dz} \qquad (15)$$

In the case of water evaporation, the diffusion coefficients D_{gas} and D_{vapour} which are applicable respectively to the thermally energized air molecules and the free evaporated water molecules are only slightly different: for O_2 molecules diffusing through air this has been measured to be 20.3 10-5 m^2s-1, compared with 24.2 10-5 m^2s-1 for H_2O. Because convection is often the significant transport process when compared with diffusion, Bowen argued that the transport of water molecules and of thermally excited air molecules in air under normal conditions would be affected in the same way, thus equalizing their transport rate, and enabling differences of molecular diffusion rates to be disregarded. It is then possible to express the ratio of the heat losses by conduction and by evaporation in terms of the ratio of the thermal energy gradient to the (postulated) latent-heat energy gradient. This is a valuable simplifying concept since, for all practical applications, the thermal losses are adequately described by a simple Newtonian model and the classical gas law.

The energy densities employed for practical applications [9] of (14) and (15) are the boundary values at the liquid surface (τ_L, ϕ_L)) and in the ambient gaseous environment (τ_A, ϕ_A).

The ratio of the total thermal-conduction and latent-heat losses defined in (13) as the Bowen Ratio now becomes

$$B = H/\lambda = d\tau / d\phi \qquad (16)$$

The simplified parameters of Equations (14) and (15) then enables estimates to be made of the rate of evaporation.

The evaluation of $d\phi/dz$ requires the water vapour density gradient ρ'_v normal to the surface,

$$\rho'_v = \frac{d\rho_v}{dz} \tag{17}$$

The ideal gas law for a vapour of molecular weight M is

$$p_V = \rho_V \frac{R}{M} T \tag{18}$$

With (17), this gives the water vapour pressure gradient:

$$p'_v = \frac{dp_v}{dz} = \rho'_v \frac{R}{M(H_2O)} T \tag{19}$$

The latent heat energy density gradient λ modelled by Bowen in (15) is consequently for SI units

$$\lambda = \rho'_v L_E = \frac{M(H_2O)\, p'_v\, L_E}{RT} \quad (J/m^4) \tag{20}$$

Similarly, the thermal energy density gradient arising from heat loss by conduction to the ambient air is

$$H = \rho_{air}\, c_p\, p_{air} \frac{dT}{dz} = p_{air} \frac{\overline{M}_{air}}{RT} c_p \frac{dT}{dz} \quad (J/m^4) \tag{21}$$

where the specific heat of air at constant pressure (c_p = 1.01 J/g K for dry air) is little affected by humidity. The ratio of thermal energy loss to latent-heat energy loss defines the dimensionless Bowen Ratio of (16):

$$B = \frac{H}{\lambda} = \frac{\overline{M}_{air}\, p_{air} C_p}{M(H_2O) L_E} \frac{dT/dz}{dp_v/dz} \tag{22}$$

The mean molecular mass of air $\overline{M_{air}}$ = 29 and $M(H_2O)$ = 18, so that

$$B = \frac{H}{\lambda} = \frac{p_{air} C_p}{0.62\, L_E} \frac{d\theta}{dp_v} = \gamma \frac{T_S - T_A}{p_v(T_S) - p_v(T_A)} \tag{23}$$

where γ = 67 Pa/K is the psychometric constant at standard air density. T_S is the temperature of the evaporation surface, T_A is the ambient temperature and $p_v(T)$ is the saturation pressure of water vapour at a temperature T. Values of the Bowen ratio B are calculated in Appendix 2.A as functions of T_S and T_A.

C. Previous Applications of The Bowen Ratio

As indicated earlier, existing applications of the Bowen ratio are normally concerned either with the rate of water loss by evaporation (e.g., from reservoirs, agricultural areas or oceans) or with the efficiency of any cooling system which utilises water evaporation. In these applications, the input data are relatively simple to acquire for the surface and air temperatures, the air pressure, and (from hygrometer measurements) the vapour pressures near the surface of evaporation and in the environment. The value of B is then obtained from (23). A low value of B corresponds to significant evaporation with a large P_E loss, as would exist for example from a water surface to a warm, dry-air environment with low vapour pressure e_A. For example, sea-water evaporation at low latitudes is very high and corresponds with a Bowen Ratio of about 0.1, whereas at 70°N the value is about 0.45. It is notable that even the latter higher value indicates that the rate of evaporative heat loss is more than double that of conductive cooling.

The next Section will consider the new application of this concept to the thermal modelling of contaminated insulators in a moist environment in order to quantify this significant contribution of evaporation loss to voltage gradient distortion.

V. APPLICATION OF THE THERMAL MODEL TO POLLUTED INSULATORS

A. The Inclusion of The Latent Heat Loss by Evaporation in The Heat Loss Function $f\,[\theta(x)]$

The magnitude of the Bowen Ratio in the leakage-current heat loss from a polluted insulator will vary over its surface because the temperature rise $\theta(x)$ with respect to the environment varies along the insulator. For each surface location, the same five parameters are needed to determine this variable B(x) as was the case in the applications of Section IV.C. In fog-chamber tests, the three ambient parameters of the enclosure (the air pressure p, fog temperature T_A and vapour pressure p_A) will have a common value for all surface locations x on the insulator. The fog is assumed to have the relevant saturated vapour pressure at T_A, namely $p_A = p_v(T_A)$. At the insulator surface, the variation of temperature $T_S(x)$ is obtained by infrared imaging (Section II). Evaporation occurs at all locations x, so that the saturation vapour pressure close to the warmer surface can also be assigned a higher value $p_v(T_S(x))$. With the evaluation of B(x) ((23) and Appendix 1.B), it then becomes possible to complete the calculation of the heat loss function $f[\theta(x)]$ as the combined steady-state power loss/unit area by radiation, conduction, convection and evaporation with Eqs. (6, 7, 10 and 13):

$$\begin{aligned} f[\theta(x)] &= P_I(x) = P_H(x) = P_{CC}(x) + P_E(x) + P_R(x) \\ &= [\, h\,(1 + 1/B(x)) + 4\,\varepsilon\,\sigma\, T_A^3\,]\,\theta(x) \\ &= h\, f_1(x) + f_2(x) \end{aligned} \tag{24}$$

B. The Modified Voltage Gradient $E_m(X)$

The component values $f_1(x)$ and $f_2(x)$ of the heat loss function in (24) can be calculated for each point on the insulator creepage path from the measured $\theta(x)$ and T_A data using the appropriate values of the Bowen ratio evaluated in Appendix 2.A. The values of the Newton heat transfer coefficient h which are appropriate to the sheds and trunk sections of the insulator could be obtained from a prior thermal calibration by experiment or modelling. Alternatively, as shown below, the measurement of the insulator leakage current I_L at a test voltage U was possible in the present fog tests and enables a value of the heat transfer coefficient h for the trunk sections to be obtained as follows. The input power loss/unit area $P_I\{Tr\}$ on a trunk section of length T and diameter D between adjacent sheds of an insulator before the formation of dry bands is shown in Appendix 1 to be

$$P_I\{Tr\} = \frac{UI_L}{F(\pi D)^2} \tag{25}$$

Appendix 1 also shows that the input power loss/unit area after dry band formation is significantly increased to a value

$P_{DB}\{Tr\}$ which will usually be different for each trunk section. Then, the value of the heat transfer coefficient $h\{Tr\}$ for any trunk section of the insulator is obtained using the mean values, over that trunk length T, of the heat loss functions f_1 and f_2 of (24):

$$h\{Tr\} = f[\theta(x)\{Tr\}] = \frac{P_{DB}\{Tr\} - f_2\{Tr\}}{f_1\{Tr\}} = \frac{P_{DB}\{Tr\} - \frac{1}{T}\int_0^T f_2(x)dx}{\frac{1}{T}\int_0^T f_1(x)dx} =$$

$$= \frac{T\,P_{DB}\{Tr\} - \int_0^T f_2(x)dx}{\int_0^T f_1(x)dx} \quad (26)$$

A numerical evaluation of $h\{Tr\}$ from (26) that will have a common value for each trunk uses (A.9 – A.11) (Appendix Equations), and requires the data of the thermal profile $\theta(x) = (T_S(x)-T_A)$ for all trunk sections, the leakage current I_L and the test voltage U. An application of this procedure is given in Section V.C.

The profile of the modified voltage gradient (using (5) and (24)) along each trunk length T can then be obtained from

$$E_M(x) = \frac{h\,f_1(x) + f_2(x)}{F\,\overline{E(x)}\,I_L} \quad (27)$$

A verification of the reliability of the thermal model is obtained from an integration of $E_M(x)$ over the creepage distance L of the insulator including sheds, since this should equate to the test voltage U:

$$\int_0^L E_M(x)dx = U = \int_0^L \frac{f[\theta(x)]}{F\,\overline{E(x)}\,I_L}\,dx \quad (28)$$

As indicated earlier, a prior knowledge of the heat transfer coefficient h would enable both the leakage current I_L and the profile of the modified voltage gradient $E_M(x)$ to be obtained from the thermal data.

C. Case Study for the Calculation of the Voltage Gradient Modification Caused by Dry Bands

This modelling has been verified using standard laboratory clean-fog tests of silicone rubber composite insulators with various saline pollution densities, in tests designed to include IR time-resolved photography. The dry bands at the trunk sections of the insulator are shown by the model to cause voltage gradients to be up to fourfold greater than the undistorted values. Such measured gradients of 250-400 kV/m are fully consistent with the streamer channels that are observed to bridge and stabilise the bands, and which prevent rewetting prior to the appearance of partial arcs.

Figure 2 illustrates the test insulator of Table I. Figures 3(a) and (b) are examples of simultaneous visible and infrared records of the formation of a pair of dry bands in a fog chamber test. The latter record provides the temperature measurement of the fog environment T_A and of the insulator axial temperature profiles $T_S(x)$. Together with the current characteristics, these data inform the computation procedure described in Table II below and the application of the thermal model to the test data. Columns 1 – 5 of the procedure of Table II use both these data and the undistorted field distribution before dry-band formation (3) along the creepage distance of the insulator (375mm). Columns 6 – 11 of Table II will be the output values obtained from the thermal modelling of (25)-(28) of the dry-band formation. Finally, column 11 of Table II will quantify the modification of the voltage gradient E_M (x) by dry band formation in this case study.

The numerical application of the Table II procedure to a fog chamber test example of temperature, current and voltage data is available as additional file (link).

(a) Visible dry-band streamers

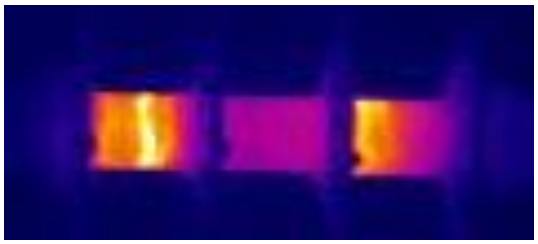

(b) Infrared record of dry-bands

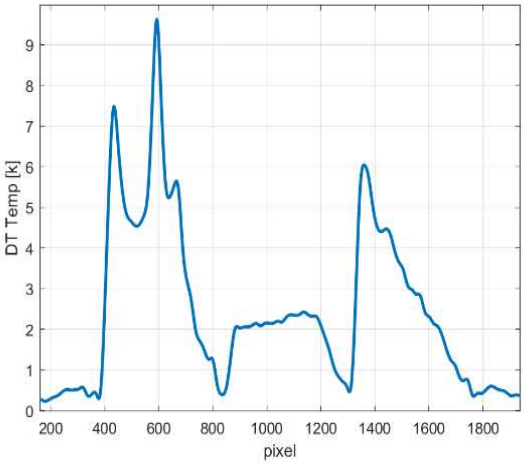

(c) Surface temperature heating $T(x) = T_S - T_A$

Fig. 3. Fog test of polluted insulator. U = 18.4kVrms, Leakage current I_L = 0.22 mA.

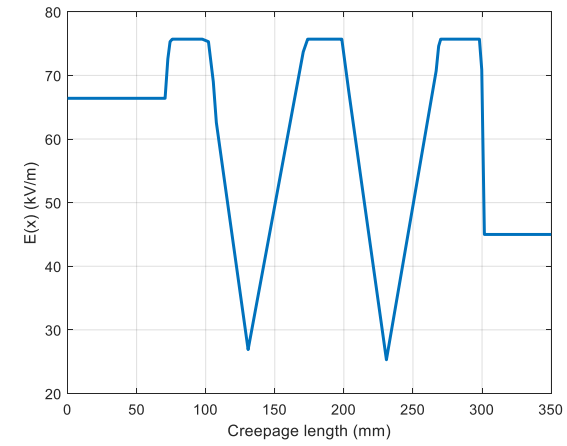

a)

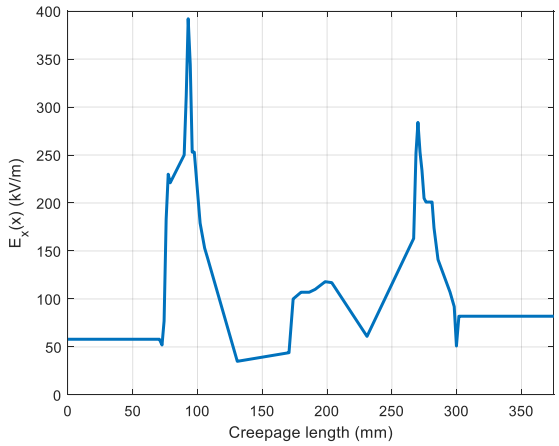

b)

Fig. 4. Undistorted electric fields $E_x(x)$ (a) and distorted E_M (x) (b) along the insulator creepage length; Data and computation: additional file (link).

TABLE II

THERMAL MODELLING: COMPUTATION PROCEDURE

Column	Description
1	Axial distance from HV termination of test insulator (0 -175mm)
2	Creepage distance from HV termination of test insulator (0 – 375mm)
3	Per-unit voltage gradient $\overline{E(x)}$ (m^{-1}) without dry-band formation (Eq. (3))
4	Voltage gradient E(x) (kV/m) at U=18.4kV without dry-band formation
5	Pollution layer temperature data $T_S(x)$ K (T_A = 288.1K)
6	Bowen ratio from Figure A.1
7	Evaluation of f_1 ($\theta(x)$, T_A) from (24) and (26) ($\theta(x) = T_S(x) - T_A$)
8	Evaluation of f_2 ($\theta(x)$, T_A) from (24)
9	Numerical integration of $\int_0^L f_2(\theta(x), \theta_A)dx$ with intervals of creepage distance x from Column 2 $*\ \int_0^L f_1(\theta(x), \theta_A)dx = \sum Column\ 9 = 1.27\ \mathrm{K.m}$
10	Numerical integration of $\int_0^L f_2(\theta(x), \theta_A)dx$ with intervals of creepage distance x from Column 2 $**\int_0^L f_2(\theta(x), \theta_A)dx = \sum Column\ 10 = = 2.29\ W/m$ *** Evaluation of heat transfer coefficient h (trunk) from (A.7, A.8))
11	Evaluation of voltage gradient $E_M(x)$ at 18.4kV as modified by dry-band formation (Equation (27): plotted profile of Figure 4 **** Verification of (28) by numerical integration of $\int_0^L \frac{f[\theta(x)]}{F\,\overline{E(x)}\,I_L}dx = U$

*** h (trunk) = 34 $W/m^2/K$

**** U (trunks) = 16.5kV
U (sheds and end sections) = 1.9kV

The full details available in the additional file (link)

VI. CONCLUSION

A viable thermal model of leakage-current power loss in polluted insulators during moist conditions is possible only if accompanied by a quantitative estimation of evaporation losses from the insulator. This has been achieved here with the Bowen concept to quantify the aqueous evaporation rate. Although the concept has been widely used in other disciplines, it has not hitherto been employed in high-voltage technology before. This has enabled the model to show that evaporation heat loss from a wetted insulator surface is two to four times greater than that associated with conduction or convection. Because such evaporation causes dry bands to form readily and inevitably on moist polluted insulators, insulator designs must control the large voltage differences across these bands in order to inhibit the consequent risk of partial arcing which is damaging to polymeric insulators.

The model allows infrared temperature data to quantify the distortion by dry bands of the voltage gradient along the creepage path of the insulator which may initiate damage by partial arcing.

The insulator leakage current associated with dry banding is in the milliampere range and could be estimated online by the model. The technique is being further developed to derive from infrared data the larger leakage current magnitudes of several hundred milliamperes associated with partial arcs observed in laboratory tests which can ensue from severe dry banding. This will provide opportunities for quantitative online condition monitoring of insulation integrity and of power losses in difficult environments.

APPENDIX 1 HEAT TRANSFER COEFFICIENT ESTIMATION

The test insulators of the present work (Section II) have three trunk sections each of creepage distance T = 35mm, four sheds of diameter 50mm, and two end trunk sections of lengths 23 and 28mm. These will respectively have corresponding creepage distances on the equivalent cylinder of T_e = 54mm, S_e = 33.5mm, and E_e = 35.5 and 43.5mm. This enables the per-unit voltage difference across each of the trunks, and sheds of the insulator itself can thus be obtained:

$$U\{T\}(pu) = \frac{T_e}{L} = \frac{T}{\pi FD} = 0.144 \text{ pu} \quad (A.1)$$

$$U\{S\}(pu) = \frac{S_e}{L} = 0.089 \text{ pu} \quad (A.2)$$

A further combined U{E}(pu)=0.212 pu voltage difference occurs across trunk end-sections. The per-unit voltage gradient across each insulator trunk is

$$E\{T\}(pu) = \frac{U\{Tr\}(pu)}{T} = 4.11 \text{ m}^{-1} \quad (A.3)$$

and the mean per-unit voltage gradient across each insulator shed is

$$E\{Sh\}(pu) = \frac{U\{Sh\}(pu)}{S} = 0.71 \text{ m}^{-1} \quad (A.4)$$

where S = 125mm is the surface creepage distance of the insulator between trunk sections.

The thermal analysis of Section V.B uses $P_I\{Tr\}$ to represent the power loss per unit area from a trunk section of area A{Tr} with a pollution layer of conductance k. Before the formation of a dry band, this is (from A.2) of area A[T] with a pollution layer of conductance k.

$$P_I\{Tr\} = \frac{U\{T\}(pu) U I_L}{A\{T\}} = \frac{U I_L T}{F\pi D} \cdot \frac{1}{\pi D T} = \\ = \frac{U I_L}{F (\pi D)^2} = 46.8 \text{ U } I_L \text{ W/m}^2 \quad (A.5)$$

This compares with a significantly lower mean value of $P_I\{Sh\} = 7.75 \text{ U } I_L \text{W/m}^2$ on a shed surface.

A power dissipation per unit area which is sufficient to cause dry band formation on a trunk section is immediately followed by streamer discharges which bridge the dry surface of the band. These both maintain a reduced leakage current and maximize the power dissipation on that trunk section. The pre-dry-band value of (A.5) is no longer valid because the power dissipation is determined by the streamer characteristics, and dry-band formation on heavily polluted insulators is invariably observed at low voltages. If the terminal voltage U is sufficient to initiate higher current partial-arcs across the band (Figure 1(c)), significant transient peaks of the leakage current and power dissipation will follow.

The observed absence of dry bands on the shed surfaces on this insulator is clearly a consequence of the pre-band condition $P_I\{Tr\} = 6P_I\{Sh\}$ as described above. This difference becomes even greater in dry-band conditions. However, if high-current partial-arc channels are initiated in a trunk section, these may bridge the adjacent sheds.

The combined leakage resistance of the sheds and end-trunks in present tests (Section II) has been calculated from (A.2) to be 0.568MΩ, and this will be unaffected by dry bands which are usually seen to develop only across the inter-shed trunk sections in the fog tests. On the other hand, the dry-band trunk resistances $R_{DB}\{Tr\}$ will be significantly greater. Therefore, in this case, we have the sum of the three trunk resistances as

$$\sum_1^3 [R_{DB}\{Tr\}]_n = \frac{U}{I_L} - 0.568 \text{ M}\Omega \quad (A.6)$$

The total power per unit area which is dissipated by dry band activity on three trunk sections of total area 3A{Tr} is thus

$$\sum_1^3 [P_{DB}\{Tr\}]_n = \frac{I_L^2 \sum_1^3 [R_{DB}\{Tr\}]_n}{3A\{Tr\}} = \frac{I_L(U - 0.568 I_L)}{3\pi DT} \quad (A.7)$$

This estimate can now be related to the thermal model of Section V.B Equation (26), which allows the common value of the heat transfer coefficient h to be obtained for the trunk sections:

$$h = \frac{T \sum_1^3 [P_{DB}\{Tr\}]_n - \sum_1^3 [\int_0^T f_2[\theta(x), \theta_A] dx]_n}{\sum_1^3 [\int_0^T f_1[\theta(x), \theta_A] dx]_n} \quad (A.8)$$

where $f_1[\theta(x), \theta_A]$ and $f_2[\theta(x), \theta_A]$ are the components of the heat loss function $f[\theta(x)]$ in (24). The profile of the modified electric field $E_M(x)$ can then also be obtained from these components (Eq.(27), as shown in Figure 5 (Section V.C).

APPENDIX 2 BOWEN RATIO EVALUATION

The values for B, as defined in (23), are shown in Figure A.1. These have been calculated using the SVP data in Table A.I.

TABLE A.I

SATURATED VAPOUR PRESSURE $P_V(T)$ FOR WATER

T (°C)	10	15	20.0	25	30	35	40
p_v (T) (kPa)	1.23	1.72	2.35	3.25	4.30	5.65	7.60

The importance of evaporation power loss is clear from Figure A.1 where for a surface temperature T(x) which is only slightly above an ambient temperature of 20°C, the Bowen Ratio value indicates that the power loss by evaporation from the insulator surface is three times that by conduction and becomes increasingly so at higher $\theta_S = T(x) - T_A$.

The evaporation rate R from the insulator surface can be obtained from (A.9)

$$R = \frac{P_{CC}}{BL_E} \quad (A.9)$$

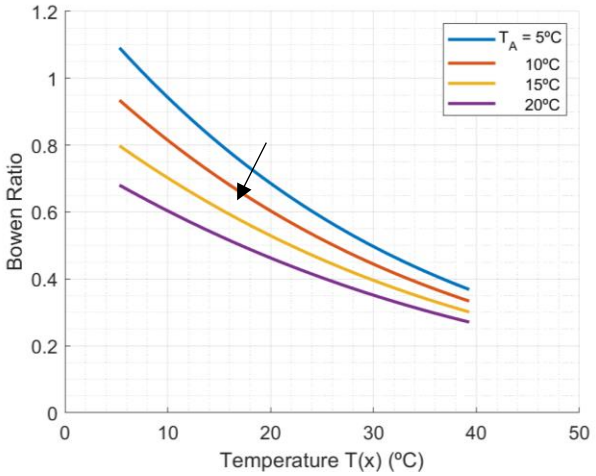

Fig. A.1. Bowen ratio of conduction and evaporation heat losses. T_A = Ambient temperature. T(x) = Insulator surface temperature (at creepage location x)

ACKNOWLEDGMENT

Authors thanks Chris Stone for the technical support and the assistance in longtime exposure photography during the laboratory tests.

REFERENCES

[1] M. Albano, R.T. Waters, P. Charalampidis, H. Griffiths and A. Haddad, 2016, "Infrared analysis of dry-band flashover of silicone rubber insulators", *IEEE Trans. Dielectr. Electr. Insul*. 23, No. 1, pp 304-310.

[2] S.F. Stefenon, R. Bruns, A. Sartori, L.H. Meyer, R.G. Ovejero and V.R. Q. Leithardt, 2022, "Analysis of the Ultrasonic Signal in Polymeric Contaminated Insulators Through Ensemble Learning Methods," in *IEEE Access*, vol. 10, pp. 33980-33991, doi: 10.1109/ACCESS.2022.3161506.

[3] I. Bowen, 1926, "The ratio of heat losses by conduction and by evaporation from any water surface", *Physical Review*, 27, pp 779-787,

[4] P. Charalampidis, M. Albano, H. Griffiths, A. Haddad and R.T. Waters, 2014, "Silicone rubber insulators for polluted environments part 1: enhanced artificial pollution tests," *IEEE Transactions on Dielectrics and Electrical Insulation*, vol. 21, no. 2, pp. 740-748, doi: 10.1109/TDEI.2013.004015.

[5] M. Albano, P. Charalampidis, R.T. Waters, H. Griffiths and A. Haddad, "Silicone rubber insulators for polluted environments part 2: textured insulators," 2014, *IEEE Transactions on Dielectrics and Electrical Insulation*, vol. 21, no. 2, pp. 749-757, doi: 10.1109/TDEI.2013.004016.

[6] M. Knudsen, 1934, "The Kinetic Theory of Gases: some modern aspects" (London: Methuen,).

[7] S.S. Penner, 1952, 'On the kinetics of evaporation', Physical Review 56, 475-450

[8] J.P. Holman, "Heat Transfer", 2002, Mc Graw Hill, Ninth Edition, New York, 665 pg

[9] W.J. Shuttleworth, "Terrestrial Hydrometeorology", 2012, Wiley-Blackwell, 1st edition, 472 pg. ISBN: 978-0-470-65937-3.

Maurizio Albano (Member, IEEE) Maurizio Albano received his 5-year degree (M.Eng.) in 1999 and then the Ph.D. degree in electrical engineering from the University of Padova, Italy in 2003. In 2006 he joined the Advance High Voltage Engineering Research Centre at Cardiff, and he is now Senior Lecturer at Cardiff University. His present fields of research are insulation co-ordination, air insulated compact substations, electromagnetic fields computation, Artificial Intelligence applied on monitoring techniques and overhead line insulator design.

Dr Albano is a Member of IEEE and IET. He is member of BS PEL36 and IEC TC 36 Insulators working group PT 63414.

Ronald T. Waters received the Ph.D. degree at University of Wales, Swansea in 1954. He researched at AEI, Aldermaston, UK with teams on nuclear fusion, high speed photography, electron microscopy and high voltage technology. From 1963, his university work at Cardiff initiated international collaborations in high voltage engineering and gaseous breakdown, including participation with the European Les Renardieres Group on UHV phenomena. He has been closely associated since 1972 with the biennial International Symposium on High Voltage Engineering of which he is a Steering Committee member.

Prof Waters is a Fellow of IET (formerly IEE, UK) and is now Emeritus Professor at Cardiff University.

Mohammed El Amine Slama. (Member, IEEE), was an Assistant Professor with the University of Lyon 1, Villeurbanne, France, from 2010 to 2011, a Lecturer with the University of Sciences and Technology of Oran (USTO), Bir El Djir, Algeria, and a member of the High Voltage and Electrical Field Team, Laboratory of Electrical Engineering, USTO, Algeria, from 2004 to 2008 and from 2011 to 2013). He was a Researcher with the SuperGrid Institute, Villeurbanne, and General Electric, Lyon, France, from 2014 to 2017. He was a Researcher with the Advanced High Voltage Engineering Research Centre (AHIVEC), Cardiff University, Cardiff, U.K. He is currently Senior Research Engineer at IRT Saint Exupéry, France. He has authored or coauthored more than 100 scientific articles and technical reports. His main research interests include outdoor insulation, flashover and breakdown in gases, eco-friendly gases for SF_6 replacement, high-voltage (HV) insulation and engineering, HV power system protection, and insulation coordination.

Dr. Slama is a member of BSI PEL036, IEC-TC 36/PT, and IEEE DEIS Outdoor Insulation Technical Committee and a reviewer for several international journals.

A. Manu Haddad (Member, IEEE) obtained the degree of Ingénieur d'Etat in electrical engineering in 1985 and then a Ph.D. degree in High Voltage Engineering in 1990 at Cardiff University, where in 2006 he was appointed Professor in electrical engineering with responsibility for the High Voltage Energy Systems Group (HIVES). His research interests are in overvoltage protection, insulation systems, insulation coordination and earthing of electrical energy systems. He has co-authored an IET-Power Series Book on "Advances in High Voltage Engineering".

Prof Haddad is a member of IET, CIGRE, British Standard Institution committees: BSI PEL1 and PEL2, the International Electrotechnical committees IEC TC37 MT4 and MT10, and IEC ACTAD. He is currently the Chair of IEC TC37 committee.